An expanded palette of fluorogenic HaloTag probes with enhanced contrast for targeted cellular imaging

Sylvestre Bachollet, Yuriy Shpinov, Fanny Broch, Hela Benaissa, Arnaud Gautier, Nicolas Pietrancosta, Jean-Maurice Mallet, Blaise Dumat

An expanded palette of fluorogenic HaloTag probes with enhanced contrast for targeted cellular imaging

Sylvestre P.J.T. Bachollet,[a] Yuriy Shpinov,[a] Fanny Broch,[a] Hela Benaissa,[a] Arnaud Gautier,[a,b] Nicolas Pietrancosta,[a,c] Jean-Maurice Mallet[a] and Blaise Dumat[a]*

[a] Laboratoire des biomolécules, LBM, Département de chimie, École normale supérieure, PSL University, Sorbonne Université, CNRS, 75005 Paris, France.

[b] Institut Universitaire de France (IUF), 1 rue Descartes, 75005 Paris

[c] Neuroscience Paris Seine - Institut de Biologie Paris Seine (NPS - IBPS) INSERM, CNRS, Sorbonne Université, Paris, France.

*Corresponding author : blaise.dumat@ens.psl.eu

Abstract

We report the development of HaloTag fluorogens based on dipolar flexible molecular rotor structures. By modulating the electron donating and withdrawing groups, we have tuned the absorption and emission wavelengths to design a palette of fluorogens with emissions spanning the green to red range, opening new possibilities for multicolor imaging. The probes were studied in glycerol and in presence of HaloTag and exhibited good fluorogenic properties thanks to a viscosity-sensitive emission. In live-cell confocal imaging, the fluorogens yielded only a very low non-specific signal that enabled wash-free targeted imaging of intracellular organelles and proteins with good contrast. Combining experimental studies and theoretical investigation of the protein/fluorogen complexes by molecular dynamics, these results offer new insight into the design of molecular rotor-based fluorogenic HaloTag probes in order to improve reaction rates and the imaging contrast.

Keywords: Fluorogenic probes; molecular rotors; HaloTag; Fluorescence imaging

Introduction

Fluorescence imaging has become an invaluable tool to study the structure and dynamics of living systems due to its high sensitivity (down to the single molecule), high temporal and spatial resolution and to its biocompatibility, allowing non-invasive imaging of samples in physiological conditions. Numerous fluorescent molecular probes have been developed over time and organic chemistry offers virtually endless possibilities to tailor fluorophores for each application.[1] Nonetheless, since the discovery of the Green Fluorescent Protein (GFP), fluorescent proteins (FPs) have taken a prominent place in the field of bioimaging thanks to the unparalleled targeting selectivity of genetic encoding. A large variety of FPs has since been developed with emission spanning the whole visible spectrum and optimized optical and biochemical properties paving the way to multicolor and complex imaging experiments.[2] More recently, hybrid chemogenetic systems have appeared, that associate a genetically encoded self-labeling protein tag with a small molecular fluorophore linked either covalently or non-covalently to the protein.[3–7] Such combination benefits from the genetic targeting of FPs and from the structural diversity and versatility of organic chromophores and it offers better spatial and temporal control over the fluorescent labeling compared to fluorescent proteins that are continuously expressed and fluorescent. It may nonetheless suffer from common problems associated with molecular probes, including the risk of off-target binding, yielding non-specific signal, and the need to wash the excess of dye. To alleviate these issues, advanced chemogenetic reporters are built on fluorogenic probes that only become fluorescent when bound to the cognate protein tags.[8–11] Considerable efforts have thus been put in the development of fluorogens with diverse optical properties and on their association with protein tags, in particular the most commonly used SNAP-tag[12–15] and HaloTag.[16–21] The latter is, to date, one of the most useful tag for covalent protein labeling with high selectivity and fast reaction kinetics. Its chemically simple and lipophilic chloroalkane ligand also facilitates the synthesis of the dedicated probes as well as their cell permeability.[22]

The HaloTag is derived from a bacterial alkane dehalogenase and was built and optimized (up to the last iteration HaloTag7) to bind xanthene dyes and especially rhodamine derivatives with high reaction rates (k_2 = 1.9 x 10^7 $M^{-1}s^{-1}$ for TMR-Halo at 25°C).[3,23] This has driven a lot of the research on HaloTag probes towards rhodamines and, more particularly, fluorogenic Si-Rhodamines taking advantage of the polarity-sensitive spirocyclization reaction.[19,20,22,24–26] This approach certainly yields highly efficient fluorescent chemogenetic reporters but has narrowed their chemical diversity. Alternative strategies to develop fluorogenic HaloTag probes have relied on the intrinsic viscosity and/or polarity-sensitive emission of dipolar fluorophores.[16,17,27] The approach was pioneered by Kool and coworkers who developed a dimethylamino-styrylpyridinium dye with a viscosity-sensitive emission that was activated upon reaction with HaloTag thanks to the immobilization inside the protein binding channel.[17] These "molecular rotor" structures allow exploring a much wider chemical space: the fluorescence activation mechanism is applicable to a large variety of dipolar structures with electron-donating and withdrawing groups connected through a flexible conjugated bond and is commonly used to develop biomolecular probes.[28–33] Based on this strategy, we have previously reported a series of red and far-red emitting fluorogenic HaloTag probes (Figure 1A).[21] After reaction with HaloTag, the probes are covalently tethered to the protein and exhibit large enhancements of their fluorescence emissions compared to their free form in water (up to 156-fold). The two most promising fluorogens **Red-Halo2** and **NIR-Halo1** enabled wash-free imaging of the nucleus and actin in live cells by targeting HaloTag-NLS and HaloTag-LifeAct fusion proteins respectively. We nonetheless observed a low nonspecific signal in the cytoplasm that may prove detrimental when imaging low-abundant or cytosolic proteins.

Herein, taking advantage of the versatile design, we report an expanded palette of HaloTag fluorogens designed to cover a wider emission range from green to red and to minimize the non-specific signal. The new set of probes was characterized *in vitro* by absorption and fluorescence spectroscopies and in cellular imaging by confocal microscopy. Some new analyses were also performed on the previously reported **Red-Halo2** and **NIR-Halo1** probes for comparison purposes. The photophysical properties were studied *in vitro* in glycerol and in presence of HaloTag to confirm their viscosity-dependent emission and fluorogenic reaction with the protein tag. The selectivity of the probes in wash-free imaging experiments was then studied in cells and, taking advantage of the superior contrast of the newly designed probes, we applied them to image of a variety of cellular organelles and proteins.

Results and discussion

Design and synthesis. The previously reported Red-Halo and NIR-Halo probes cover an emissive range from red to far-red. In order to cover a lower wavelength range, we have modified **Red-Halo2** to introduce two lesser deficient electron-withdrawing groups, 2-cyanoacetic acid or imidazolinone, to form, respectively, the green and yellow emitting derivatives **CCVJ-Halo** and **Y-Halo** (Figure 1B). 2-Cyanoacetic acid gives the CCVJ fluorophore which is a classical molecular rotor with a green emission used as a fluorogenic protein probe and presents a readily available carboxylic acid function for conjugation with the HaloTag ligand.[13,34,35] CCVJ was already coupled to HaloTag but with a different ligand unit which does not readily make the probe fluorogenic upon reaction and was instead used to detect protein aggregation.[27] Imidazolinone is the electron withdrawing group found in the GFP chromophore and, in aminated derivatives, it was reported to afford yellow-emitting compounds.[36,37]

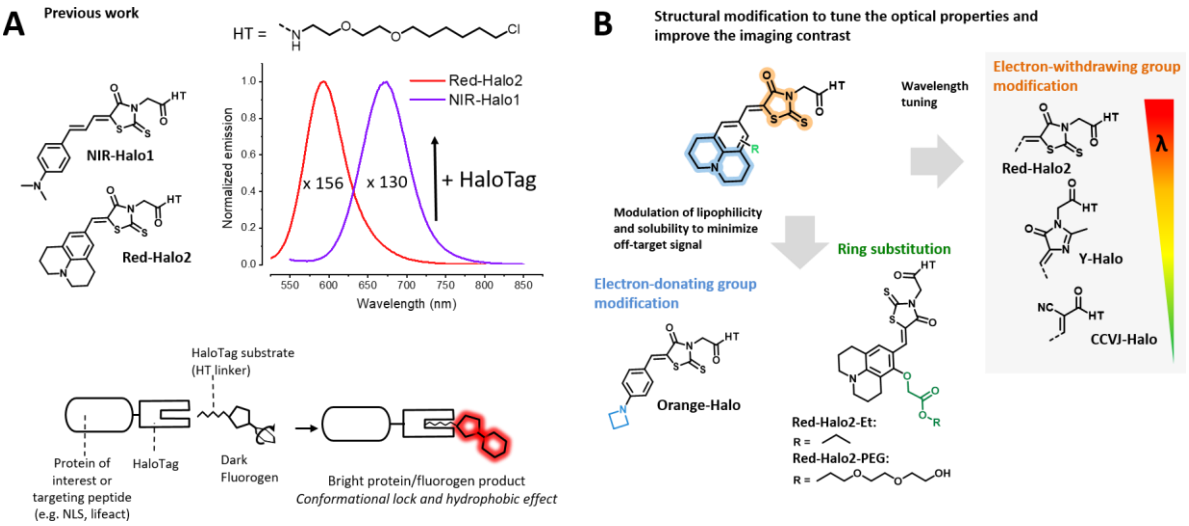

Figure 1. Design and structures of the fluorogenic HaloTag probes.
(A) structures of two of the previously reported probes with their fluorescence emission spectra and fluorescence enhancement upon reaction with HaloTag and general schematic description of the fluorogenic reaction with HaloTag. (B) Structural modifications and structures of the new probes.

In addition to the emission color-tuning, the second goal was to minimize the unspecific signal observed with **Red-Halo2** and **NIR-Halo1** due to the partial activation and/or accumulation of the fluorogens in cytoplasmic organelles. Factors governing the non-specific binding of a dye to intracellular components are difficult to predict and depend in part on the net charge (*e.g*. positively charged compounds binding to mitochondria) and on the lipophilic/hydrophilic balance. The Halo dyes are neutral structures with poor water solubility and we hypothesized that their lipophilic character is one of the driving force of the non-specific binding by leading the probes to accumulate into lipid structures such as the endoplasmic reticulum (ER) membrane. We have thus set out to develop analogs of **Red-Halo2** with lower lipophilicity. As a first strategy, we substituted the aniline ring of **Red-Halo2** with an ethyl or a triethyleneglycol chain through an ester coupling to afford **Red-Halo2-Et** or **Red-Halo2-PEG** respectively (Figure 1B). The ethyl ester is expected to induce only a minute decrease in the lipophilicity of **Red-Halo2**, thanks to the polar ester function, while the addition of a PEG chain is known to increase the hydrophilicity. In a second approach, we have introduced an azetidine donating amino group instead of the julolidine (Figure 1). Azetidine was previously reported as an efficient locked amino donating group since the 4-membered cycle strain prevents the formation of a "twisted intramolecular charge transfer" (TICT) state and it may advantageously replace julolidine while being slightly less lipophilic.[20] Azetidine is also less electron-donating than julolidine and yielded the blue-shifted orange-emitting **Orange-Halo**. Using inexpensive building blocks and reagents, the probes can be obtained in straightforward 2 to 4 steps synthetic procedures detailed in the supplementary information (Scheme S1-S4).

Photophysical properties and reaction with HaloTag. With their flexible dipolar structures, all probes display typical molecular rotor features and we have previously evidenced the fluorogenic behavior of **Red-Halo2** and **NIR-Halo1** in presence of proteins.[21] We have nonetheless confirmed the molecular rotor properties (*i.e.* the viscosity-dependent emission) for the whole series of probes (of the two ester derivatives **Red-Halo2-PEG** and **Red-Halo2-Et**, only the latter was studied) by measuring their spectral properties in water and in glycerol (Figure S1 and Table 1). As expected from the rational design, all probes are weakly fluorescent in water but their emission is strongly enhanced (from 28 to 390-fold) in glycerol with quantum yields ranging from 9 to 20 %, in accordance with an increase in viscosity (Table 1). The largest fluorescence enhancement in glycerol is observed for **Orange-Halo** and is due to the combination of a shift in the excitation wavelength with the fluorescence activation: although the azetidine is slightly less electron-donating than the julolidine, **Orange-Halo** is expected to have spectral properties close to those of **Red-Halo2** but its absorption in water is unexpectedly blue-shifted (409 nm). In glycerol however, a large bathochromic shift is observed resulting in an

absorption spectrum more akin to the parent **Red-Halo2** (Figure S1, Table 1). The solubility in water was assessed by UV-vis absorption spectroscopy. Between 0.5 and 20 µM, the probes obey the Lambert-Beer law with the exception of Red-Halo2-Et and NIR-Halo1 which show solubility limit around 13 µM and 1 µM respectively (Figure S2A&B). Beyond a 1 µM concentration, the absorption spectrum of NIR-Halo1 exhibits a sharp blue-shifted absorption band that may be attributed to aggregation as is observed for H-aggregates in cyanine dyes (Figure S2C). The unexpectedly blue-shifted absorption of Orange-Halo in aqueous buffer may suggest that it also forms soluble aggregates, but the transition between the free and aggregated form is not visible in the studied concentration range. The viscosity-sensitive emission and good fluorescence brightness observed in glycerol confirm the potential of the probes to be used as fluorogenic biomolecular probes and we next studied the reaction of the probes with a GST-HaloTag (GST-HT) protein *in vitro* and the resulting fluorescence properties of the formed complexes (Figure 2 and Table 1).

Table 1. Photophysical properties of the Halo probes in glycerol and in presence of HaloTag.
λ_{abs} and λ_{em}: maximum absorption and emission wavelength, ε: molar absorptivity coefficient, *FWHM*: Full width at Half maximum of the emission spectrum, Φ_F: fluorescence quantum yield, $\varepsilon \cdot \Phi_F$: brightness, k_2: second order reaction rate constant, F/F_0: Fluorescence enhancement factor where F and F_0 are the integrated fluorescence intensities in glycerol or HaloTag and in water respectively.

Molecule	Solvent/ target	λ_{abs} (nm)	ε (10^3 $M^{-1}cm^{-1}$)	λ_{em} (nm)	FWHM (nm)	Φ_F	$\varepsilon \cdot \Phi_F$	k_2[c] (10^3 $M^{-1}s^{-1}$)	F/F_0
CCVJ-Halo	Glycerol	455	33.9	495		0.19	6441		129
	HaloTag[a]	458	31.8	498	54	0.014	445	1.0 ± 0.1	15
	buffer	443	22.7	505					
Y-Halo	Glycerol	487	26.2	556		0.099	2594		28
	HaloTag[a]	489	34.9	562	50	0.015	524	n.d.	12
	buffer	483	24.3	548					
Orange-Halo	Glycerol	486	15.2	578		0.14	2128		390
	HaloTag[a]	487	16.2	574	64	0.020	324	0.45 ± 0.03	48
	buffer	413	18.5	590					
Red-Halo2-Et	Glycerol	520	14.9	595		0.086	1281		32
	HaloTag[a]	504	14.5	588	65	0.050	725	0.29 ± 0.04	32
	buffer	490	14.7	601					
Red-Halo2-PEG	HaloTag[a]	525	32.7	599	61	0.055	1800	5.3 ± 0.3	22
	buffer	530	14.4						
Red-Halo2[b]	Glycerol	521	22.9	602		0.20	4580		298
	HaloTag[a]	515	21.0	592	60	0.17	3600	1.3 ± 0.2	156
	buffer	483	14.8	609					
NIR-Halo1[b]	Glycerol	527	27.5	664		0.091	2503		225
	HaloTag[a]	526	25.8	671	68	0.053	1400	1.7 ± 0.04	130
	buffer	480	22.8	684					

[a]Measurement conditions: 1 µM dye with 1.3 µM GST-HT in pH 7.4 phosphate buffer containing 10 mM Phosphate and 100 mM NaCl. [b]Data taken from reference 21 except for k_2 values. [c]Average of duplicate experiments.

All probes undergo a fluorogenic reaction reaction with GST-HT, which allowed us to measure the reaction rate constants by following the increase of fluorescence over time (Figure 2A&B). With the exception of **Y-Halo**, the reactions obey a classical pseudo-first-order exponential law and the calculated second order reaction rate constants are comprised between 0.29 10^3 and 5.3 10^3 $M^{-1}s^{-1}$ (Table 1). The slowest reaction rates were observed for **Orange-Halo** and **Red-Halo2-Et** which can be explained in part by solubility issues: the more hydrophilic **Red-Halo2-PEG** displays the fastest reaction rate, an order of magnitude higher than that of its ethyl ester counterpart. The possible aggregation of **Orange-Halo** in water may also explain its slow reaction kinetics. The reaction with **Y-Halo** is almost instantaneous with an immediate sharp increase of fluorescence that is followed by a slower decrease of intensity that stabilizes after a few minutes (Figure 2B). It is possible that **Y-Halo** undergoes a first non-covalent association with the protein yielding a highly fluorescent complex followed by the covalent enzymatic reaction that leads to a compound with lower fluorescence. Alternatively, it may also adopt several conformations with different emissive properties once bound to the protein. Apart from **Y-Halo**, the reaction rates of the probes are slower than that of rhodamine-based HaloTag ligands but they are in the same range or faster than that observed for other reported solvatochromic HaloTag probes[16,18] and for alternative self-labeling protein tags such as SNAP-tag, CLIP-tag and PYP-tag.[4,5,10,12]

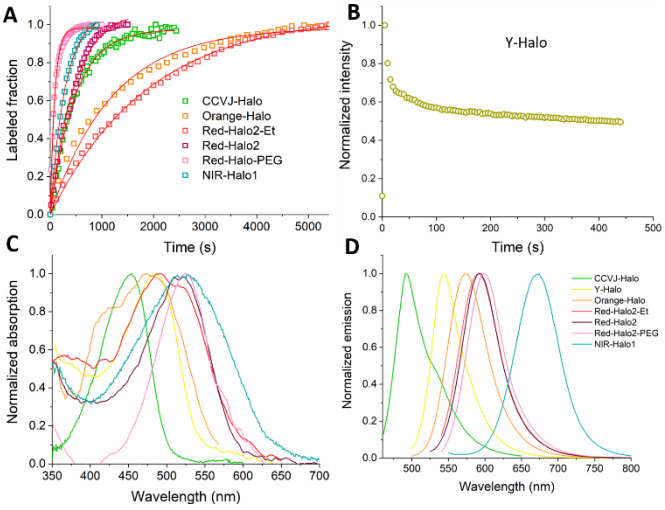

Figure 2. Reaction of the Halo probes with GST-HaloTag.
(A,B) Reaction kinetics of the Halo probes with GST-HT. [dye] = 100 nM, [GST-HT] = 2 µM, T = 298 K. Data was fitted to an exponential rise function (red lines) with the exception of Y-Halo. Normalized absorption (C) and emission (D) of the Halo probes bound to HaloTag. [Dye] = 1 µM, [GST-HT] = 1.3 µM.

After reaction with HaloTag, the spectral properties of the bound probes are essentially similar to those in glycerol but with lower fluorogenicities (Figure 2C&D, Table 1). **CCVJ-Halo** and **Y-Halo** display comparable 12 to 15-fold fluorescence activation and while **Red-Halo2-Et, Red-Halo2-PEG** and **Orange-Halo** perform slightly better, the five new probes have lower fluorescence enhancement factors than their parent compound **Red-Halo2** (156-fold). These lower values are due to their lower fluorescence brightnesses but also, for some compounds and in particular **Y-Halo**, to higher residual fluorescence in water (Figure S3). Despite a similar fluorescence activation mechanism, the probes display large differences in fluorogenicities and fluorescence quantum yields that do not correlate with the relative properties observed in glycerol (Table 1). The green and yellow probes in particular are dimmer in HaloTag than in glycerol and the two-step binding reaction of **Y-Halo** may for instance indicate that, of several possible conformations within the protein, the most stable is not necessarily the most emissive.

Molecular dynamics. To better understand the properties of the hybrid reporters, we performed molecular dynamics on the fluorogen/HaloTag complexes over 1 ns with a 10 ps step, generating 100 poses that were clustered to identify representative structures of the various possible conformations (Figure 3 and Figure S4). Similar calculations were previously performed for **Red-Halo2** and **NIR-Halo1**.[21] The calculations yielded at least two clusters for each complex, showing that the fluorogens are indeed able to adopt several conformations within HaloTag. The results also highlight that the probes have few interactions with the protein and remain in contact with the solvent. Consequently, they retain an important structural mobility as evidenced by the RMSF values of the fluorogen moieties (Figure 3). The main interaction between HaloTag and the fluorogens occurs with the F144 residue via π-stacking with the aniline ring or with the electron-withdrawing group. That interaction is however not always favorable and can lead to twisted non-planar conformations that are not favorable for fluorescence emission. Overall, these observations explain the differences in properties observed between glycerol and HaloTag: the probes are not fully immobilized within the protein and there is only a partial activation due to viscosity and hydrophobic effects on the surface of the protein. This partial activation was relatively efficient for **Red-Halo2**, with little difference between HaloTag and glycerol but less so for other derivatives and in particular for **CCVJ-Halo**, **Y-Halo** and **Orange-Halo**. This suggests that the optimization of the interaction with HaloTag, through variation of the ligand length and/or mutation of the binding site, may lead to much brighter complexes.

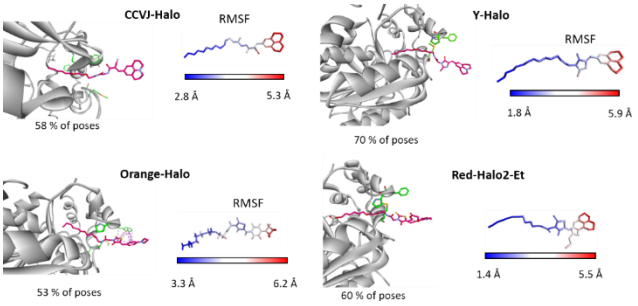

Figure 3. Molecular dynamics of the HaloTag/fluorogen complexes.
Representative structures of the major conformation cluster and root mean square fluctuations "RMSF" of the structures.

Biophysical and photophysical characterization in cellular imaging. Even with a targeted fluorogenic probe, some nonspecific signal is inevitable and can arise from the spontaneous accumulation and partial activation of the excess probe in cellular organelles with a favorable hydrophobic environment and/or increased viscosity (*e.g.* ER, membrane). This non-specific signal will grow stronger with the probe concentration but will also depend on the relative amount of expressed HaloTag protein which will vary from one experiment to another depending on the transfection level. Some cytosolic signal can also originate from the specific reaction of the probe with newly synthesized proteins not yet addressed. To demonstrate the applicability of our HaloTag fluorogens, we evaluated and compared their selectivity and imaging contrast in wash-free live-cell imaging experiments.

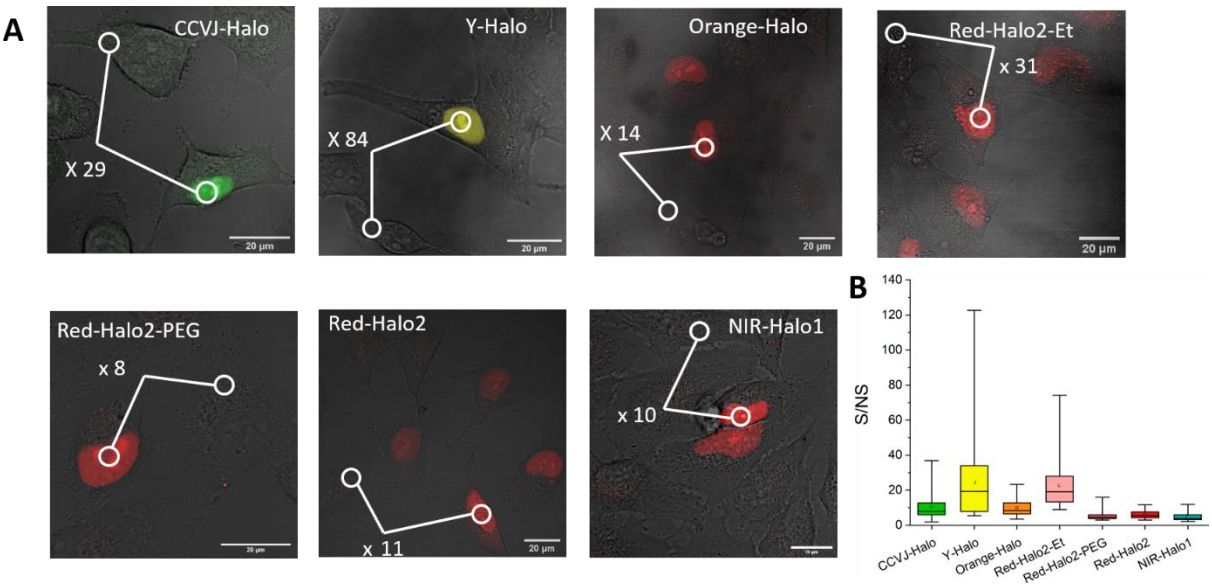

Figure 4. Selectivity and contrast of the Halo probes in cellular imaging.
(A) Live confocal imaging of Hela cells transiently expressing a HaloTag-NLS protein and incubated with 0.5 µM of fluorogenic Halo probe. On each panel is displayed the contrast ratio between the average nuclear intensity and the average cytoplasmic signal measured in a non-transfected cell. λ_{exc} = 514 nm except for CCVJ-Halo (458 nm) and Y-Halo (488 nm). Scale bar: 20 µm (B) Ratio of the specific (S = average intensity in the nucleus) over the non-specific signal (NS = averaged intensity in a cytosolic region of a non-transfected cell). Box and whiskers plot with center lines and squares showing the median and average values for n cells respectively. Box delimits the 25th and 75th percentiles and the whiskers show the max and min values. CCVJ-Halo: n = 64 from four experiments, Y-Halo: n = 91 from three experiments, Orange-Halo: n = 91 from three experiments, Red-Halo2- Et: n = 94 from four experiments, Red-Halo2-PEG: n = 92 from two experiments, Red-Halo2: n = 54 from three experiments, NIR-Halo1: n = 72 from four experiments.

Hela cells transiently expressing the HaloTag-NLS protein were stained with 0.5 µM of Halo probe and were imaged after 30 to 60 minutes without washing steps or medium change. After incubation, the cells showed a good viability with no sign of cytotoxicity and all four new probes were successful in selectively staining the nucleus (Figure 4A). For each fluorogen, we have compared the specific signal (S) in the nuclei with the non-specific signal (NS) in the cytoplasm of an adjacent untransfected cell. The contrast ratio (S/NS) is given on each

panel of figure 4A. For a more precise analysis, we have calculated the contrast on a larger set of cells from several independent experiments and the distribution of the results is given as a box plot (Figure 4B and Table S1). The specific signal (and thus the related contrast) is highly dependent on the expression level from one cell to another, which causes a large dispersion of the values, but average and maximum contrast values inform on the relative performance of the probes. Amongst the **Red-Halo2** analogs, the azetidine derivative **Orange-Halo** and **Red-Halo2-Et** give an improved contrast compared to the parent compound **Red-Halo2** but not the more hydrophilic **Red-Halo2-PEG.** These observations are confirmed by the comparison of the fluorescence signal generated by each analog in wild-type Hela cells under identical imaging conditions (Figure S5). **Red-Halo2-PEG** yields the same non-specific cytoplasmic signal as **Red-Halo2** while that of **Orange-Halo** and **Red-Halo2-Et** is respectively 3 and 6-fold lower which is well in line with the relative distribution of the S/NS ratios. The diverging properties of **Red-Halo2-PEG** (higher brightness, faster reaction but lower imaging contrast) and **Red-Halo2-Et** (slower reaction and higher contrast) show that the substitution of the aniline ring is a promising but not easily rationalized strategy to improve the properties of the Halo probes. And, contrary to our initial assumption, the non-specific fluorescence signal in cells is not directly or at least not only linked to the hydrophilic/lipophilic balance of the probes. The green and yellow emitting derivatives, **CCVJ-Halo** and **Y-Halo** also exhibit improved S/NS ratios that reach remarkably high values for the latter. **Y-Halo** yields almost no recordable unspecific signal which, despite its moderate brightness once bound to HaloTag, makes it a very promising fluorogenic reporter. To further evidence the increased contrast of the new probes we have successfully carried out wash-free imaging with the two most promising probes **Y-Halo** and **Red-Halo2-Et** at higher concentrations of 1 and 5 µM (Figure S6). At 1 µM, both probes still yield very contrasted images and, at 5 µM, the nonspecific signal becomes visible but the contrast remains satisfactory. These results stress the difficulty of designing efficient fluorogenic probes and the necessity to balance *in vitro* and cellular properties: a high fluorescence enhancement factor *in vitro* is an important figure of merit for a fluorogen, yet it does not always translate into a high contrast in cellular imaging. Here, despite its superior optical properties measured in cuvette, **Red-Halo2** is also the most prone to off-target activation in cells yielding a higher non-specific signal. On the other hand, the new probes, with the exception of **Red-Halo2-PEG**, exhibit improved contrast values that are not directly correlated to the relative brightness or fluorescence enhancement values measured *in vitro*. We finally investigated the photostability of the probes in confocal microscopy and compared it to that of Halo-TMR, a commercial tetramethylrhodamine fluorescent HaloTag ligand. Under continuous illumination for 10 to 15 minutes, the HaloTag fluorogens exhibited a good photostability which appears related to the nature of the electron withdrawing group. All compounds derived from **Red-Halo2** with a rhodanine group suffered higher photobleaching while the CCVJ and imidazolinone derivatives exhibited an excellent photostability higher than that of Halo-TMR (Figure 5). The poorest photostability was observed for **NIR-Halo1**, which can be explained by the extended π-system and the presence of a dimethylamino electron-donating group instead of the julolidine. Overall, the HaloTag fluorogens are robust fluorophores able to sustain high excitation intensities with low photobleaching, which compensates partly for their moderate brightness.

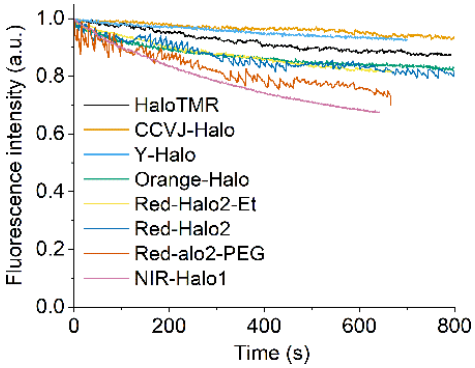

Figure 5. Photostability of the HaloTag fluorogens. Evolution of the normalized intensity in the nuclei of Hela cells transfected with HaloTag-NLS and incubated with 0.5 µM of HaloTag fluorogens under continuous illumination for 10 to 15 minutes. The photostability of Halo-TMR was also measured for comparison purposes.

Targeted subcellular imaging. In order to take advantage of their increased contrast, we have used the palette of novel HaloTag probes to image of variety of cellular components in addition to the nuclear labeling discussed above (Figure 6 and Figure S7).

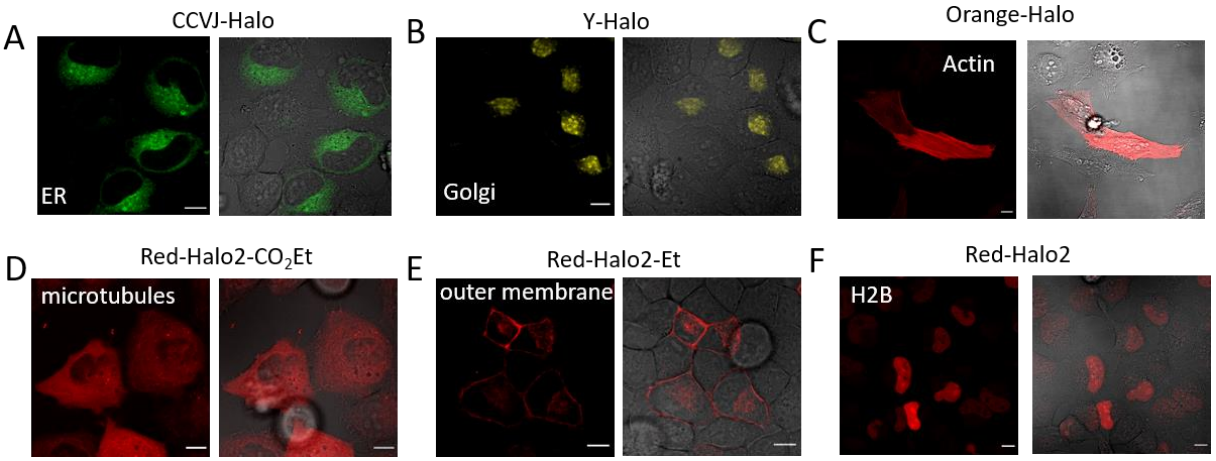

Figure 6. Targeted organelles and proteins imaging.
Live wash-free confocal imaging of Hela cells transiently expressing H2B-HaloTag (nucleus), MAP4-HaloTag (microtubules), PDGFR-HaloTag (external membrane), ER-HaloTag (endoplasmic reticulum), HaloTag-Lifeact (actin) or Golgi-HaloTag (Golgi apparatus) and incubated with 0.5 µM of CCVJ-Halo (A), Y-Halo (B) or Orange-Halo (C) Red-Halo2-Et (D,E) and Red-Halo2 (F). Each panel diplays the fluorescence image (left) and the merged fluorescence and brightfield images (right). Non-transfected cells are visible on the merged images to evidence the selective labeling. λ_{exc} = 514 nm except for CCVJ-Halo (458 nm) and Y-Halo (488 nm) Scale bar: 10 µm.

The parent compound **Red-Halo2** remains efficient to image the nucleus via the targeting of Histone 2B or the cytoskeleton (microtubules). Although microtubule bundles are clearly visible, the labeling of microtubules using MAP4-HaloTag also yielded a significant cytoplasmic signal (Figure 6D and Figure S7). The plasmid is derived from the MAP4-FAST plasmid that generated a satisfactory microtubules labeling[8] and it is possible that the larger HaloTag protein interferes with the microtubule binding. Except for this limitation, the new fluorogens proved successful in imaging the endoplasmic reticulum (ER), the golgi apparatus, H2B, the outer membrane and actin. In addition to providing a wider range of excitation and emission wavelength, the new probes, thanks to their improved selectivity, enabled the imaging of additional cellular targets, including cytoplasmic organelles.

Multicolor imaging. CCVJ-Halo, **Y-Halo** and **Orange-Halo** display absorption spectra centered on 458 nm, 489 nm and 487 nm respectively, which allows for an optimal excitation with the 458 and 488 nm Argon laser lines commonly available on microscopes. The **Red-Halo2** derivatives and **NIR-Halo1** can be efficiently excited with the 488 or 514 nm laser lines. Due to their flexible structures that increase the number of available vibrational energy levels, the Halo probes inherently display broad emission peaks. The more flexible structure **NIR-Halo1** displays the broadest peak, with a FWHM of 68 nm and the emission peaks of the **Red-Halo2** analogs have comparable, albeit slightly narrower, breadth (Table 1). Although considerable progress has been made in the analysis and spectral deconvolution of multicolor images, these large emission ranges may render their discrimination from other fluorophores more difficult in multiplexed experiments. On the other hand, the green and yellow derivatives, **CCVJ-Halo** and **Y-Halo**, exhibit narrower emission peaks with FWHM of 54 and 50 nm that could make them more easily applicable in multicolor imaging. As an example, we have successfully combined **Y-Halo** and Mitotracker Deep Red FM in Hela cells expressing Halo-NLS (Figure 7). Both probes can be selectively excited and their emission collected without any cross-talk.

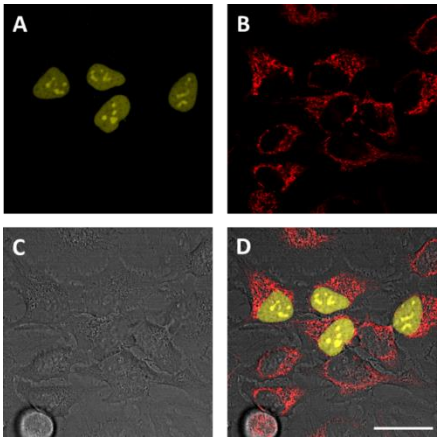

Figure 7. Multicolor imaging.
Live confocal imaging of Hela cells expressing HaloTag-NLS and incubated with 100 nM of Mitotracker Deep Red FM and 0.5 µM of Y-Halo. (A) yellow channel λ_{exc} = 488, collection: 495 – 600 nm, (B) red channel λ_{exc} = 633, collection: 640 – 799 nm, (C) transmission and (D) composite image. Scale bar: 30 µm.

Conclusion

The fluorogenic HaloTag probes reported here enrich a palette of hybrid chemogenetic reporters with good photostability, low nonspecific signal and diversified spectral properties that cover the green to far-red emission range. Despite these promising results, comparison with glycerol and theoretical studies show that the molecular rotors are only partially activated after reaction with the protein by lack of a defined hydrophobic binding pocket. Recent reports suggest that discrete mutations of HaloTag may be performed to better fit solvatochromic or molecular rotor probes.[18,38] In parallel to rational molecular design, engineering of the HaloTag protein may thus be envisioned to improve the association with the fluorogens and reach higher quantum yields and faster reaction kinetics.

Experimental procedures

Probes synthesis and characterization. Detailed synthetic procedures and chemical analyses are available in the supplementary information.

Photophysical properties with HaloTag. The fluorogenic dyes were dissolved in DMSO at a stock concentration of 0.5 mM. The interaction of the probes with Halotag was assessed by incubating the dye at 1 µM (0.4 µL of stock solution) concentration with 1.3 µM (ca. 6 µL of commercial stock solution) of protein in a 200 µL working volume of pH 7.4 Phosphate buffer (10 mM phosphate with 100 mM NaCl). Fluorescence spectra were recorded at regular time intervals until completion of the reaction. The different photophysical properties of the protein-bound probes were then measured.

Kinetics study of the labeling reactions. The second-order rate constants of the reactions were calculated by monitoring the fluorescence intensity during the reaction of the probes with a large excess of protein to assume a pseudo first-order kinetics law according to the following procedure.
GST-HT (2 µM) was added to a 50 µL solution of Halo probe (100 nM) in pH 7.4 Phosphate buffer (10 mM Phosphate, 100 mM NaCl). The fluorescence intensity (excitation and emission at the maximum absorption and emission wavelengths of each probe) was then recorded over time until completion of the reaction with a 5 s to 20 s step depending on the probe. The second order rate constants were then calculated according to a previously reported model:[7] the fluorescence was converted to the labeled fraction according to the following equation:

$$Labeled\ fraction = (F-F_0)/(F_{max}-F_0)$$

Where F_{max} and F_0 are the maximum and initial fluorescence intensity respectively. Using Origin 2019 software, the data was fitted to the following equation to calculate the pseudo first-order rate constant k_{obs}:

$$Labeled\ fraction = 1 - exp(-k_{obs}t)$$

The second order rate constant k_2 was then obtained by dividing k_{obs} with the protein concentration.

Molecular dynamics. Molecular dynamics are performed using similar conditions than previously described.[21] Briefly, 3D models of HaloTag coupled to the fluorogen compounds were generated based on a 3D structure of Halotag (pdb entry: 4KAF), refined, minimization and equilibrated by molecular dynamics simulations (1-ns runs) using the CHARMm forcefield. Bonds involving hydrogen atoms were constrained using the SHAKE algorithm.[48] The Ramachandran plot of the final 3D model showed 88% (259/295) favored, 7% (21/295) allowed, 5% (15/295) disallowed residues for Red-Halo2-Et and, respectively, 88% (259/295), 8% (24/295), 4% (12/295) for Orange-Halo, and 85% (251/295), 11% (33/295), 4% (11/295) for Y-Halo, and 86% (265/295), 9% (28/295), 5% (16/295) for CCVJ-Halo. A solvent box with a periodic boundary of 9 Å was added to the model. Solvation was completed with 0.145 M KCl using the solvation protocol implemented in Discovery Studio (Dassault Systèmes BIOVIA, Discovery Studio, 2020, San Diego: Dassault Systèmes, 2019).

Molecular Biology. Detailed construction of the plasmids used in this study are described in the supplementary information.

Confocal microscopy. Hela cells were grown overnight on 8-well polymer µslides from Ibidi (#1.5 polymer coverslip, tissue culture treated) at 20k to 50k cells/well in 300 µL of MEM culture medium (Gibco) supplemented with 10% fcs, sodium pyruvate and non-essential amino acids. Cells were then transfected with the desired plasmid using Fugene 6 (Promega Corp.) according to the manufacturer's protocol (200 ng of DNA per well with a 3:1 fugene to DNA ratio). After 24 hours, the medium was changed and replaced with DMEM (no phenol red) and the cells were incubated 30-60 minutes with the dyes and imaged live on a Zeiss LSM710 laser scanning confocal microscope equipped with a Plan apochromat 40X/1.4 NA objective. For photostability measurements, images were acquired under a continuous illumination of 37.5 kW/cm^2 measured in the focal plane over 15 minutes at a resolution of 1024x1024 and a pixel dwell time of 0.52µs. Images were acquired using Zen 2009 software and then processed using ImageJ.

Multicolor imaging with mitotracker Deep Red FM and Y-Halo. Cells were grown according to the protocol above and then labeled Mitotracker Deep Red FM according to the manufacturer protocol. Briefly, Mitotracker was diluted at 100 nM in DMEM (no phenol red) and the cells were incubated for 30 min with the resulting solution. The medium was changed to pure DMEM and the cells were then incubated with **Y-Halo** according to the protocol above. For imaging conditions, see the caption of Figure 5.

Acknowledgements

This work was supported by the Agence Nationale de la Recherche (ANR-18-CE44-0006) and the European Research Council (ERC-2016-CoG-724705 FLUOSWITCH).

Supplementary information

Supplementary figures, materials and methods, chemical synthesis and molecular biology procedures are available in supplementary information.

References

(1) Lavis, L. D.; Raines, R. T. Bright Ideas for Chemical Biology. *ACS Chem. Biol.* **2008**, *3* (3), 142–155.

(2) Day, R. N.; Davidson, M. W. The Fluorescent Protein Palette: Tools for Cellular Imaging. *Chem. Soc. Rev.* **2009**, *38* (10), 2887–2921.

(3) Los, G. V.; Encell, L. P.; McDougall, M. G.; Hartzell, D. D.; Karassina, N.; Zimprich, C.; Wood, M. G.; Learish, R.; Ohana, R. F.; Urh, M.; et al. HaloTag: A Novel Protein Labeling Technology for Cell Imaging and Protein Analysis. *ACS Chem. Biol.* **2008**, *3* (6), 373–382.

(4) Keppler, A.; Gendreizig, S.; Gronemeyer, T.; Pick, H.; Vogel, H.; Johnsson, K. A General Method for the Covalent Labeling of Fusion Proteins with Small Molecules in Vivo. *Nat. Biotechnol.* **2003**, *21* (1), 86–89.

(5) Gautier, A.; Juillerat, A.; Heinis, C.; Corrêa, I. R.; Kindermann, M.; Beaufils, F.; Johnsson, K. An Engineered Protein Tag for Multiprotein Labeling in Living Cells. *Chem. Biol.* **2008**, *15* (2), 128–136.

(6) Hoelzel, C. A.; Zhang, X. Visualizing and Manipulating Biological Processes by Using HaloTag and SNAP-Tag Technologies. *ChemBioChem* **2020**, *21* (14), 1935–1946.

(7) Hori, Y.; Norinobu, T.; Sato, M.; Arita, K.; Shirakawa, M.; Kikuchi, K. Development of Fluorogenic Probes for Quick No-Wash Live-Cell Imaging of Intracellular Proteins. *J. Am. Chem. Soc.* **2013**, *135* (33), 12360–12365.

(8) Plamont, M.-A.; Billon-Denis, E.; Maurin, S.; Gauron, C.; Pimenta, F. M.; Specht, C. G.; Shi, J.; Quérard, J.; Pan, B.; Rossignol, J.; et al. Small Fluorescence-Activating and Absorption-Shifting Tag for Tunable Protein Imaging in Vivo. *Proc. Natl. Acad. Sci.* **2016**, *113* (3), 497–502.

(9) Bruchez, M. P. Dark Dyes-Bright Complexes: Fluorogenic Protein Labeling. *Curr. Opin. Chem. Biol.* **2015**, *27*, 18–23.

(10) Gao, J.; Hori, Y.; Shimomura, T.; Bordy, M.; Hasserodt, J.; Kikuchi, K. Development of Fluorogenic Probes for Rapid High-Contrast Imaging of Transient Nuclear Localization of Sirtuin 3. *ChemBioChem* **2020**, *21* (5), 656–662.

(11) Szent-Gyorgyi, C.; Schmidt, B. A.; Creeger, Y.; Fisher, G. W.; Zakel, K. L.; Adler, S.; Fitzpatrick, J. A. J.; Woolford, C. A.; Yan, Q.; Vasilev, K. V.; et al. Fluorogen-Activating Single-Chain Antibodies for Imaging Cell Surface Proteins. *Nat. Biotechnol.* **2008**, *26* (2), 235–240.

(12) Leng, S.; Qiao, Q.; Miao, L.; Deng, W.; Cui, J.; Xu, Z. A Wash-Free SNAP-Tag Fluorogenic Probe Based on the Additive Effects of Quencher Release and Environmental Sensitivity. *Chem. Commun.* **2017**, *53* (48), 6448–6451.

(13) Yu, W. T.; Wu, T. W.; Huang, C. L.; Chen, I. C.; Tan, K. T. Protein Sensing in Living Cells by Molecular Rotor-Based Fluorescence-Switchable Chemical Probes. *Chem. Sci.* **2016**, *7* (1), 301–307.

(14) Sun, X.; Zhang, A.; Baker, B.; Sun, L.; Howard, A.; Buswell, J.; Maurel, D.; Masharina, A.; Johnsson, K.; Noren, C. J.; et al. Development of SNAP-Tag Fluorogenic Probes for Wash-Free Fluorescence Imaging. *ChemBioChem* **2011**, *12* (14), 2217–2226.

(15) Jung, K. H.; Fares, M.; Grainger, L. S.; Wolstenholme, C. H.; Hou, A.; Liu, Y.; Zhang, X. A SNAP-Tag Fluorogenic Probe Mimicking the Chromophore of the Red Fluorescent Protein Kaede. *Org. Biomol. Chem.* **2019**, *17* (7), 1906–1915.

(16) Liu, Y.; Miao, K.; Dunham, N. P.; Liu, H.; Fares, M.; Boal, A. K.; Li, X.; Zhang, X. The Cation−π Interaction Enables a Halo-Tag Fluorogenic Probe for Fast No-Wash Live Cell Imaging and Gel-Free Protein Quantification. *Biochemistry* **2017**, *56* (11), 1585–1595.

(17) Clark, S. A.; Singh, V.; Vega Mendoza, D.; Margolin, W.; Kool, E. T. Light-Up "Channel Dyes" for Haloalkane-Based Protein Labeling in Vitro and in Bacterial Cells. *Bioconjug. Chem.* **2016**, *27* (12), 2839–2843.

(18) Kang, M.-G.; Lee, H.; Kim, B. H.; Dunbayev, Y.; Seo, J. K.; Lee, C.; Rhee, H.-W. Structure-Guided Synthesis of a Protein-Based Fluorescent Sensor for Alkyl Halides. *Chem. Commun.* **2017**, *53* (66), 9226–9229.

(19) Wang, L.; Tran, M.; D'Este, E.; Roberti, J.; Koch, B.; Xue, L.; Johnsson, K. A General Strategy to Develop Cell Permeable and Fluorogenic Probes for Multicolour Nanoscopy. *Nat. Chem.* **2020**, *12* (2), 165–172.

(20) Grimm, J. B.; English, B. P.; Chen, J.; Slaughter, J. P.; Zhang, Z.; Revyakin, A.; Patel, R.; Macklin, J. J.; Normanno, D.; Singer, R. H.; et al. A General Method to Improve Fluorophores for Live-Cell and Single-Molecule

Microscopy. *Nat. Methods* **2015**, *12* (3), 244–250.

(21) Bachollet, S. P. J. T.; Addi, C.; Pietrancosta, N.; Mallet, J.-M.; Dumat, B. Fluorogenic Protein Probes with Red and Near-Infrared Emission for Genetically Targeted Imaging. *Chem. Eur. J.* **2020**, *26* (63), 14467–14473.

(22) Wilhelm, J.; Kühn, S.; Tarnawski, M.; Gotthard, G.; Tünnermann, J.; Tänzer, T.; Karpenko, J.; Mertes, N.; Xue, L.; Uhrig, U.; et al. Kinetic and Structural Characterization of the Self-Labeling Protein Tags HaloTag7, SNAP-Tag, and CLIP-Tag. *Biochemistry* **2021**, *60* (33), 2560–2575.

(23) Encell, L. P. Development of a Dehalogenase-Based Protein Fusion Tag Capable of Rapid, Selective and Covalent Attachment to Customizable Ligands. *Curr. Chem. Genomics* **2012**, *6* (1), 55–71.

(24) Lukinavičius, G.; Reymond, L.; Umezawa, K.; Sallin, O.; D'Este, E.; Göttfert, F.; Ta, H.; Hell, S. W.; Urano, Y.; Johnsson, K. Fluorogenic Probes for Multicolor Imaging in Living Cells. *J. Am. Chem. Soc.* **2016**, *138* (30), 9365–9368.

(25) Grimm, J. B.; Muthusamy, A. K.; Liang, Y.; Brown, T. A.; Lemon, W. C.; Patel, R.; Lu, R.; Macklin, J. J.; Keller, P. J.; Ji, N.; et al. A General Method to Fine-Tune Fluorophores for Live-Cell and in Vivo Imaging. *Nat. Methods* **2017**, *14* (10), 987–994.

(26) Frei, M. S.; Tarnawski, M.; Roberti, J.; Koch, B.; Hiblot, J.; Johnsson, K. HaloTag9 : An Engineered Protein Tag to Improve Fluorophore Performance. *BioRxiv* **2021**, doi: 10.1101/2021.04.01.438024

(27) Fares, M.; Li, Y.; Liu, Y.; Miao, K.; Gao, Z.; Zhai, Y.; Zhang, X. A Molecular Rotor-Based Halo-Tag Ligand Enables a Fluorogenic Proteome Stress Sensor to Detect Protein Misfolding in Mildly Stressed Proteome. *Bioconjug. Chem.* **2018**, *29* (1), 215–224.

(28) Hoche, J.; Schulz, A.; Dietrich, L. M.; Humeniuk, A.; Stolte, M.; Schmidt, D.; Brixner, T.; Würthner, F.; Mitric, R. The Origin of the Solvent Dependence of Fluorescence Quantum Yields in Dipolar Merocyanine Dyes. *Chem. Sci.* **2019**, *10* (48), 11013–11022.

(29) Xie, X.; Zuffo, M.; Teulade-Fichou, M. P.; Granzhan, A. Identification of Optimal Fluorescent Probes for G-Quadruplex Nucleic Acids through Systematic Exploration of Mono- And Distyryl Dye Libraries. *Beilstein J. Org. Chem.* **2019**, *15*, 1872–1889.

(30) Shaya, J.; Collot, M.; Bénailly, F.; Mahmoud, N.; Mély, Y.; Michel, B. Y.; Klymchenko, A. S.; Burger, A. Turn-on Fluorene Push-Pull Probes with High Brightness and Photostability for Visualizing Lipid Order in Biomembranes. *ACS Chem. Biol.* **2017**, *12* (12), 3022–3030.

(31) Péresse, T.; Gautier, A. Next-Generation Fluorogen-Based Reporters and Biosensors for Advanced Bioimaging. *Int. J. Mol. Sci.* **2019**, *20* (24), 6142.

(32) Klymchenko, A. S. Solvatochromic and Fluorogenic Dyes as Environment-Sensitive Probes: Design and Biological Applications. *Acc. Chem. Res.* **2017**, *50* (2), 366–375.

(33) Dumat, B.; Bordeau, G.; Aranda, A. I.; Mahuteau-Betzer, F.; Harfouch, Y. El; Metgé, G.; Charra, F.; Fiorini-Debuisschert, C.; Teulade-Fichou, M.-P. Vinyl-Triphenylamine Dyes, a New Family of Switchable Fluorescent Probes for Targeted Two-Photon Cellular Imaging: From DNA to Protein Labeling. *Org. Biomol. Chem.* **2012**, *10* (30), 6054.

(34) Iwaki, T.; Torigoe, C.; Noji, M.; Nakanishi, M. Antibodies for Fluorescent Molecular Rotors. *Biochemistry* **1993**, *32* (29), 7589–7592.

(35) Goh, W. L.; Lee, M. Y.; Joseph, T. L.; Quah, S. T.; Brown, C. J.; Verma, C.; Brenner, S.; Ghadessy, F. J.; Teo, Y. N. Molecular Rotors as Conditionally Fluorescent Labels for Rapid Detection of Biomolecular Interactions. *J. Am. Chem. Soc.* **2014**, *136* (17), 6159–6162.

(36) Baranov, M. S.; Solntsev, K. M.; Baleeva, N. S.; Mishin, A. S.; Lukyanov, S. A.; Lukyanov, K. A.; Yampolsky, I. V. Red-Shifted Fluorescent Aminated Derivatives of a Conformationally Locked GFP Chromophore. *Chem. Eur. J.* **2014**, *20* (41), 13234–13241.

(37) Ye, S.; Zhang, H.; Fei, J.; Wolstenholme, C. H.; Zhang, X. A General Strategy to Control Viscosity Sensitivity of Molecular Rotor-Based Fluorophores. *Angew. Chemie Int. Ed.* **2021**, *60* (3), 1339–1346.

(38) Miró-vinyals, C.; Stein, A.; Fischer, S.; Ward, T. R.; Deliz Liang, A. HaloTag Engineering for Enhanced Fluorogenicity and Kinetics with a Styrylpyridium Dye. *ChemBioChem* **2021**, *22 (24),* 3398-3401.

Table of contents graphic